metals

MDPI

Article

Biomimetic Design of Fatigue-Testing Fixture for Artificial Cervical Disc Prostheses

Xuejin Cheng [1,2], Jia Bai [3] and Tao Wang [1,*]

[1] College of Materials Science and Technology, Nanjing University of Aeronautics and Astronautics, Nanjing 211106, China
[2] Faculty of Mechanical and Material Engineering, Huaiyin Institute of Technology, Huaian 223003, China
[3] Suzhou Changfeng Avionics Co., Ltd., Suzhou 215151, China
* Correspondence: taowang@nuaa.edu.cn

Abstract: To investigate the biomechanical performances of artificial cervical disc (ACD) prostheses, many studies have been conducted, either with cervical sections of cadavers under physiological loads or with block-like testing fixtures obeying the ASTM F2346 standard. Unfortunately, both methods are almost impossible to utilize for accurate results of lifetime anti-fatigue experiments for at least 10 million cycles due to the difficulties in cadaver preservation and great deviations of natural cervical bodies, respectively. Based on normal human cervical structural features, a novel specimen fixture was designed for testing the fatigue behavior of ACD prostheses under flexion, extension, and lateral bending conditions, with aspects of both structural and functional bionics. The equivalence between the biomimetic fatigue-testing fixture and the natural cervical sections was investigated by numerical simulations and mechanical experiments under various conditions. This study shows that this biomimetic fatigue-testing fixture could represent the biomechanical characteristics of the normal human cervical vertebrae conveniently and with acceptable accuracy.

Keywords: artificial cervical disc (ACD); specimen fixture; fatigue behavior; biomimetic

Citation: Cheng, X.; Bai, J.; Wang, T. Biomimetic Design of Fatigue-Testing Fixture for Artificial Cervical Disc Prostheses. *Metals* **2023**, *13*, 299. https://doi.org/10.3390/met13020299

Academic Editor: Alberto Campagnolo

Received: 27 December 2022
Revised: 27 January 2023
Accepted: 30 January 2023
Published: 1 February 2023

1. Introduction

Disc arthroplasty is a new surgical treatment for intervertebral degeneration and instability. Compared with traditional cervical fusion surgery, its advantages are that it restores the range of motion of the cervical spine and can lower the incidence of adjacent segment degeneration in the long term [1–4]. ACD prostheses are intended to bear alternating loads within the scope of physiology and should theoretically last for several decades in the body without failures. The life of ACD prostheses and their minimum acceptable clinical life are disputed, however. Titanium and titanium alloys are widely used in orthopedic hard tissue repair and artificial cervical intervertebral disc manufacture because of their good biocompatibility and non-toxicity [5,6]. The optimum life span has generally been demonstrated to be 80 million movements, while 10 million movements is suggested to be the ideal minimum testing cycle [7,8].

Traditional implant trials often choose a series of cervical spine specimens from cadaver donors moisturized with saline solution. Cervical spine specimens are dissected free from soft tissues, musculature, and single-segmental cervical intervertebral discs, while the ligaments and integrity of post-zygapophysial joints are carefully preserved, and then ACD prostheses are implanted for testing [9–12]. These specimen tests must be completed in a short time to avoid causing side effects in the process of the biological disintegration of cadavers [13–17]. Unfortunately, it is almost impossible to carry out a lifetime anti-fatigue experiment for at least 10 million cycles with fresh-frozen cadavers due to the time and cost limitations of cadaver preservation.

In dealing with such problems, the tests conducted by ASTM F2346 allow for the analysis of individual disc replacement devices and the comparison of the mechanical performance

of multiple artificial intervertebral disc designs in a standard model [18–23]. Specialized test fixtures have been developed by leading machine manufacturers to conduct both static and cyclic testing of ACDs following the ASTM F2346 standard in recent decades. Due to the obvious difference between these test fixtures and the natural cervical spine, the obtained data about the static and dynamic behaviors of ACD prostheses are less accurate. Therefore, the results from these tests may not directly predict in vivo performance; however, they can be used to compare the mechanical performance of different ACD prostheses [19,20].

In dealing with the ultra-high cost and inevitable data deviation of the above-mentioned testing methods, the biomimetic methodology could be a promising solution for testing ACD prostheses with better accuracy and efficiency.

The objective of this study was to design a biomimetic fatigue-testing fixture using synthetic materials similar to human cervical vertebrae for cost-effective, accurate static and dynamic tests of ACDs, to evaluate the equivalence of the stresses and deformations (i.e., range of motion) of ACDs within the designed fatigue-testing fixture, and within C5–C6 cervical spinal segments. Fatigue simulations of ACDs within C5–C6 cervical spinal segments and within the fatigue-testing fixture and fatigue experiments of ACDs within the fatigue-testing fixture were also carried out. By comparing results, the feasibility of the designed biomimetic fatigue-testing fixture can be discussed thoroughly.

2. Materials and Methods

2.1. Biomimetic Design of Fatigue-Testing Fixture

2.1.1. Structural Bionics of Fatigue-Testing Fixture

The design of the biomimetic fatigue-testing fixture is shown in Figure 1. Based on normal human cervical structural features, four epoxy blocks filled with 70 wt% hydroxyapatite powder, the same content as natural bone, were used to simulate human cervical vertebrae, as the elastic modulus of epoxy blocks is close to that of human cervical vertebrae. A metallic flexible U-plate of the fatigue-testing fixture limited the movement of blocks to simulate the function of normal human cervical ligaments and facet joints.

In terms of the size measurement and deformation properties of the C5–C6 cervical spinal segments, as shown in Figure 1, the fixture is cost-effective and reasonable, composed of a cuboid block (01), three cylindrical blocks (02–04) and a U-plate (05). Among blocks 01–04, the cylindrical blocks 02–04 are concentric, whereas the position of cuboid block 01, as the site for compressive force to be applied, can be varied to form different loading conditions. According to preliminary estimations, the thickness and width of the U-plate (05) were 1~2 mm and 30~45 mm. The length, width, and height of the cuboid block (01) were 25~35 mm, 8~15 mm, and 8~15 mm. The radius and height of the cylindrical blocks (02–04) were 10~15 mm and 8~15 mm. The distance between the center of the cylindrical blocks (02–04) and the rear end of the U-plate (05) was 45~65 mm. Using numerical simulation analysis, the fixture design was further optimized. Additionally, the lower surface of the cylindrical block (02) and the upper surface of the cylindrical block (03) were polished to meet the body's normal physiological curvature of the cervical lordosis.

The fixture was able to work with the integration prostheses and the majority of other ACD prostheses, such as Dynamic Cervical Implant (DCI), Z-braze Dynamic Fusion, and Prestige LP, as shown in Figure 1. Among various ACDs, DCI is a single-component U-shaped implant maintaining the spinal kinematics, which imposes minimum influence on the adjacent soft tissues compared with other types of prostheses [24]. The U-shaped open structure of the DCI is more favorable for the direct observation of static and dynamic behaviors during the numerical simulations of implants. Therefore, DCI (14 mm long, 16 mm wide, and 0.8 mm thick) was selected as the ACD specimen for the study of the effectiveness of the designed biomimetic fatigue-testing fixture in substitution of the natural cervical spine in static and dynamic experiments.

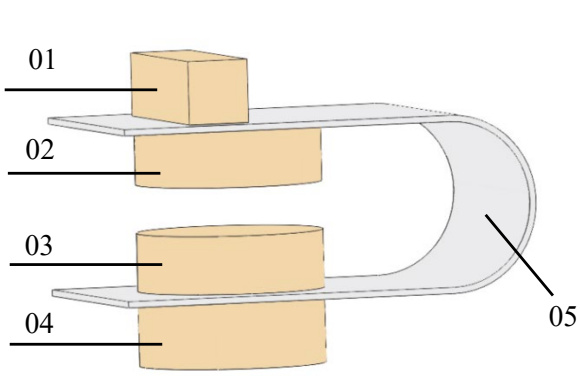

Biomimetic fatigue-testing fixture

Notes: 01 cuboid block, 02–04 cylindrical blocks, 05 U-plate

Fixture in the Instron-8874 fatigue testing

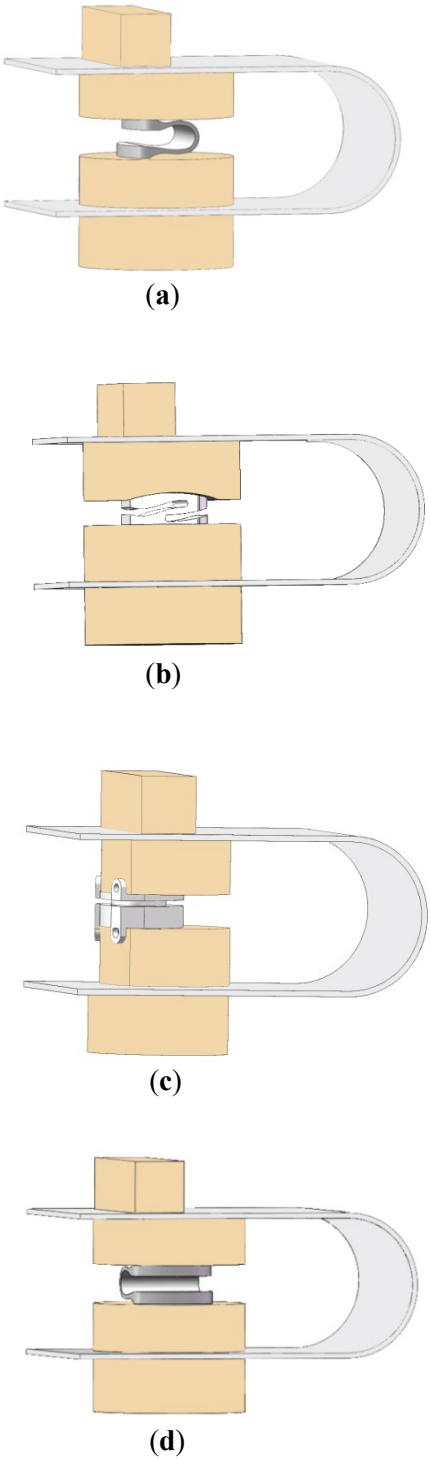

Figure 1. Assembly drawing of fixture and prostheses: (**a**) Dynamic Cervical Implants DCI under the flexion or extension condition; (**b**) Z-braze Dynamic Fusion under the flexion or extension condition; (**c**) Prestige LP under the flexion or extension condition; (**d**) DCI under the lateral bending condition.

2.1.2. Functional Bionics of Fatigue-Testing Fixture

The geometric models of the fatigue-testing fixture with DCI and the cervical bodies with DCI were established, which were input into the finite element analysis software ANSYS Workbench 16.0 (Ansys, Canonsburg, PA, USA) and assigned with corresponding material properties, as shown in Table 1 [25,26].

Table 1. Material properties of fatigue-testing fixture and spinal components used in the present model.

Description	Elastic Modulus (MPa)	Poisson's Ratio
Blocks	20,000	0.35
6061 Al alloy	70,000	0.3
Pure Ti	110,000	0.3
Ti6Al4V	110,000	0.3
Epoxy AB glue	3000	0.38
Cortical bone	10,000	0.4
Cancellous bone	100	0.29
Ligamentum flavum	1.5	0.3
Interspinous ligament	1.5	0.3
Capsular ligament	20	0.3

In the numerical calculation of the equivalent stress and deformation of DCI within the C5–C6 cervical spinal segments during the static test, the maximum routine loading parameters in biomechanical tests with cervical spines from cadaver donors were followed; namely, a 73.6 N preload was applied to the top surface of C5, with an extra 1.8 Nm flexion moment for flexion movement and a 1.8 Nm extension moment for extension or a 1.0 Nm lateral bending moment for bending, respectively, while the bottom surface of C6 was fixed in six degrees of freedom in the finite element model [26–28].

As for the simulations of the static test with the biomimetic fatigue-testing fixture, a 200 N load, the routine loading force in static and dynamic tests following ASTM F2346, was applied on the upper surface of the cuboid block 01, while the lower surface of the cylinder 04 was fixed in six degrees of freedom [19,29,30]. Furthermore, by finely adjusting the distance between the centers of DCI and the cuboid block 01, an extra equivalent moment can be obtained by multiplying the force on the top surface of the cuboid block 01 and the eccentric distance. Finally, the equivalent stress and deformation of DCI within the fatigue-testing fixture were calculated by using finite element simulation software ANSYS Workbench 16.0 (Ansys, Canonsburg, PA, USA). The equivalent stress and deformation of DCI within the fatigue-testing fixture can be made similar to those within human C5–C6 cervical spinal segments through further optimization of the parameters of the biomimetic fatigue-testing fixture.

2.2. The Process of Fatigue Simulation and Fatigue Test

The previous analysis results of DCI within C5–C6 cervical spinal segments and within the optimized fatigue-testing fixture were input into the FE-SAFE6.5 software (Dassault Systèmes Simulia Corp., Providence, RI, USA). According to the estimation methods of Seegers' material data in FE-SAFE6.5 software, SN curves were generated by inputting the tensile strength and elastic modulus, which were modified afterward [31,32]. A frequency of 10 Hz was applied with a triangular-wave load channel file. The Goodman method was used for mean stress correction, and the fatigue full-life analysis was carried out according to SN curves. After the fatigue calculation, the analysis results were re-input into ANSYS Workbench 16.0 (Ansys, Canonsburg, PA, USA) for post-processing.

In the present fatigue experiments, the DCI was fixed between the cylindrical hydroxyapatite-filled epoxy blocks 02 and 03 by epoxy AB glue in the biomimetic fatigue-testing fixture of the optimized parameters. It is used to simulate the bony fusion between the upper and lower surfaces of the DCI prosthesis and the corresponding vertebral body after the implant. The loading parameters of the cervical segment biomechanical tests were consistent with static and dynamic tests based on ASTMF2346 by adjusting the distance between the geometric center of the block and the rotating center of the artificial cervical disc. Then, the fixture, together with the DCI, was clamped between the vise and actuator of an Instron-8874 fatigue testing machine (Instron Corporation, Canton, MA, USA), as shown in Figure 1. During fatigue

experiments, the fixture was loaded with the corresponding loadings at the calculated eccentric position to provide different moments. Finally, fatigue tests were carried out until fatigue failure occurred; if not, the tests were continued until 80 million cycles were reached on the biomimetic fatigue-testing fixture.

3. Results

3.1. Optimization of the Biomimetic Fatigue-Testing Fixture

The maximum deformation of pure Ti DCI within human C5–C6 cervical segments under the flexion condition was numerically calculated as 0.57 mm, as shown in Figure 2. On the foundation that the stress of the DCI within the fatigue-testing fixture is similar to that within C5–C6 cervical spinal segments, the deformations of pure Ti DCI within the designed fatigue-testing fixture of different parameters were numerically calculated and shown in Figures 3 and 4. With the other factors being equal, the maximum deformation decreased markedly with an increase in the elastic modulus of the material and the thickness and width of the U-plate 05, respectively, as shown in Figure 3, whereas the length, width, and height of the cuboid block 01, as well as the radius and height of the cylindrical blocks 02–04, lacked an obvious influence on the DCI's maximum deformation, as shown in Figure 4a–e. Additionally, the DCI's maximum deformation increased slowly as the distance between the center of the cylindrical blocks 02–04 and the rear end of the U-plate 05 increased, as shown in Figure 4f. Likewise, the influencing tendencies of the above-mentioned factors on the deformation of DCI under the flexion condition coincide with those of DCI under either extension or lateral bending conditions. Finally, the optimizations of the various designing factors were conducted by keeping the coincidence of the stresses and deformations of the DCI within the designed biomimetic fatigue-testing fixture and within human C5–C6 cervical segments.

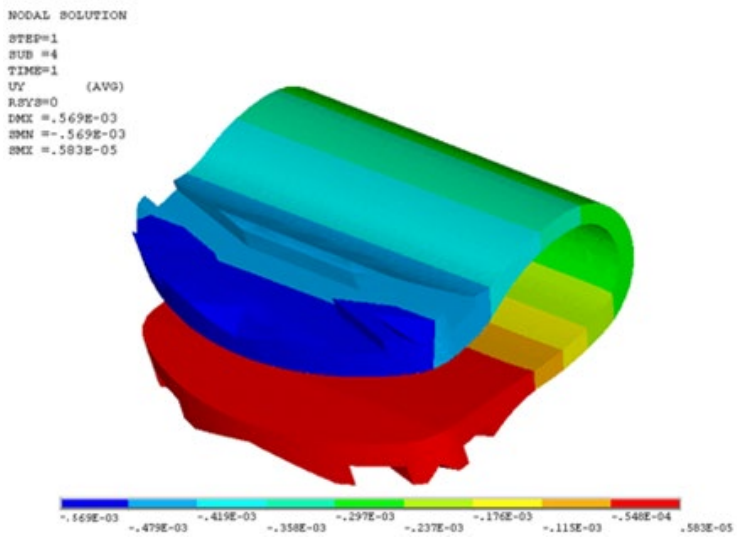

Figure 2. The deformation of pure Ti DCI within human C5–C6 cervical segments under the flexion condition.

3.2. Simulation of DCI within the Optimized Fixture under Static Mode

The contours of the equivalent stress of pure Ti DCI within the C5–C6 cervical spinal segments and within the optimized fatigue-testing fixture under the flexion condition are shown in Figure 5. The maximum equivalent stress of pure Ti DCI within the fatigue-testing fixture was 396.5 MPa, which agreed well with 394.6 MPa, the result of DCI within the C5–C6 cervical segments. More importantly, both maximum equivalent stresses appeared in the same location of the DCI. Furthermore, the contours of the equivalent stress of the DCIs of pure Ti and Ti6Al4V were simulated under various loading conditions within the fatigue-testing fixture, which were similar to those of the DCIs within the C5–C6 cervical spinal segments, as plotted in Figure 6.

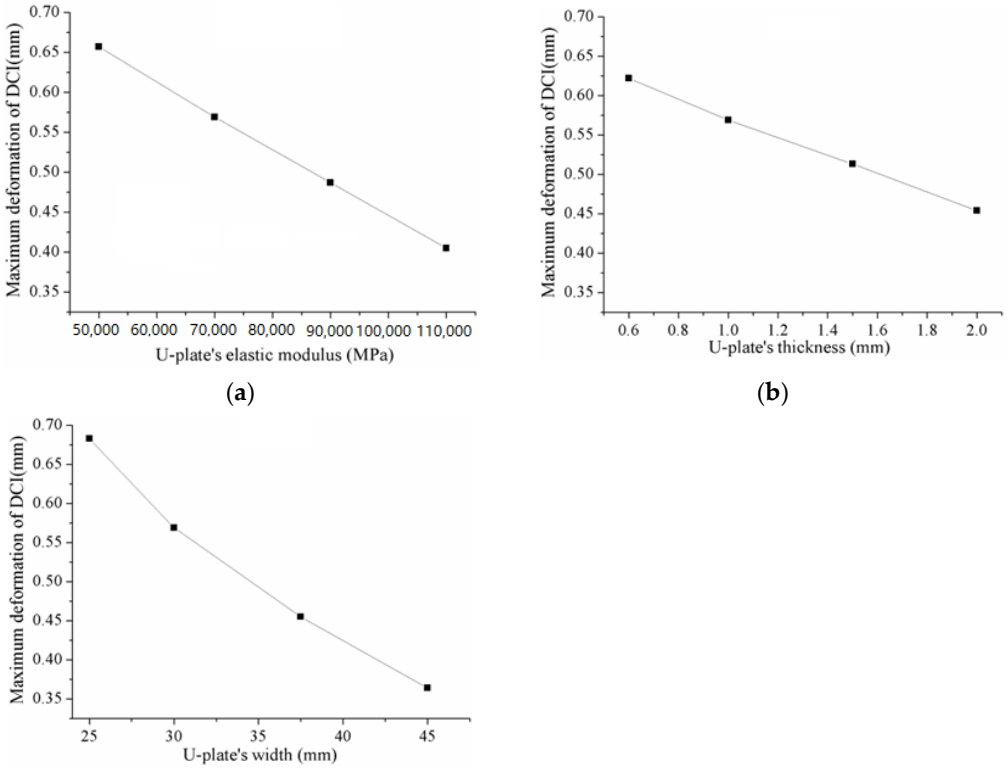

Figure 3. Influence of the U-plate's elastic modulus and size on the DCI's maximum deformation: (**a**) U-plate thickness and width were fixed at 1 mm and 30 mm; (**b**) elastic modulus and width at 70,000 MPa and 30 mm; (**c**) elastic modulus and thickness at 70,000 MPa and 1 mm.

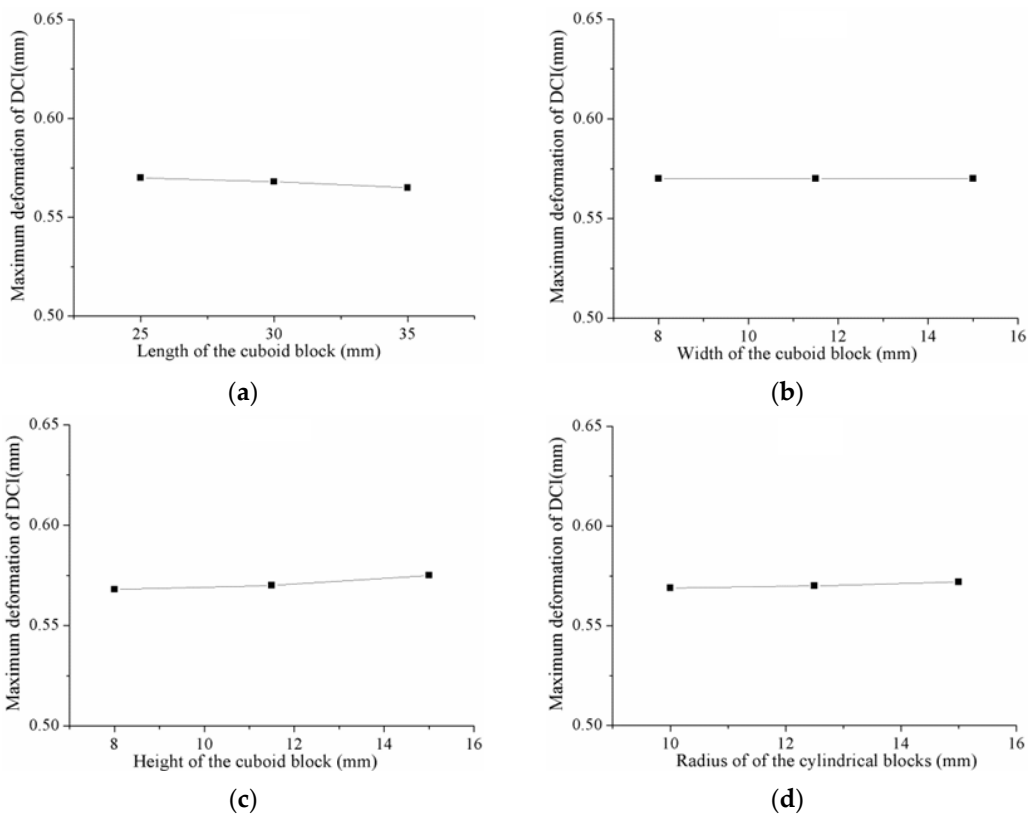

Figure 4. *Cont.*

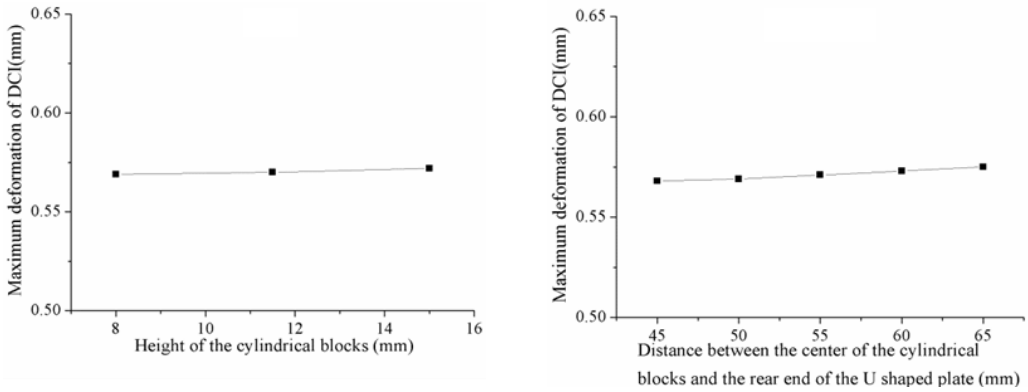

(**e**) (**f**)

Figure 4. Influence of the geometric sizes and position of the blocks on the DCI's maximum deformation: (**a**) the length of the cuboid block; (**b**) the width of the cuboid block; (**c**) the height of the cuboid block; (**d**) the radius of the cylindrical blocks; (**e**) the height of the cylindrical blocks; (**f**) the distance between the center of the cylindrical blocks and the rear end of the U-plate, assuming other factors being equal.

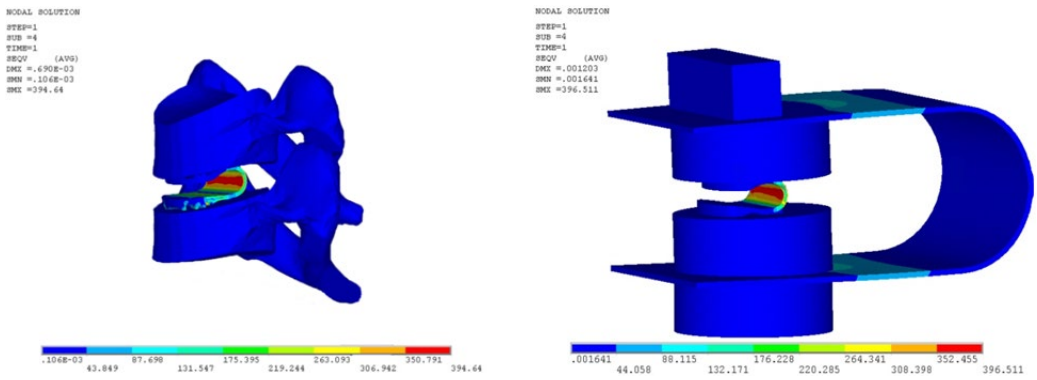

(**a**) (**b**)

Figure 5. The contours of the equivalent stress of pure Ti DCI under the flexion condition: (**a**) within C5–C6 cervical spinal segments; (**b**) within the fatigue-testing fixture.

3.3. Fatigue Simulation and Fatigue Experiment

Figure 7 shows the contours of the fatigue life of pure Ti DCI within the C5–C6 cervical spinal segments and within the optimized fatigue-testing fixture under the flexion condition. The minimums of the simulated fatigue life of pure Ti DCI within the C5–C6 cervical spinal segments and within the fatigue-testing fixture were 22.397 million cycles ($N = 10^{7.3502}$ = 22,397,000) and 21.478 million cycles ($N = 10^{7.332}$ = 21,478,000), respectively. The fatigue results of the DCIs of pure Ti and Ti6Al4V within the C5–C6 cervical spinal segments and within the fatigue-testing fixture were simulated under various loading conditions, as summarized in Table 2. The simulated fatigue life of titanium alloy exceeds 80 million cycles during flexion. In the process of extension and lateral bending, the simulated fatigue life of both pure titanium and titanium alloy exceeds 80 million times.

The fatigue-testing results of the DCIs of pure Ti and Ti6Al4V within the fatigue-testing fixture were obtained under various loading conditions by using an Instron-8874 fatigue-testing machine, as plotted in Table 2. It was shown that the experimental fatigue life of pure Ti DCI within the fatigue-testing fixture under the flexion condition was 35.645 million cycles, whereas the fatigue lives of pure Ti DCIs under other experimental conditions, as well as Ti6Al4V DCIs under all experimental conditions, were more than 80 million cycles.

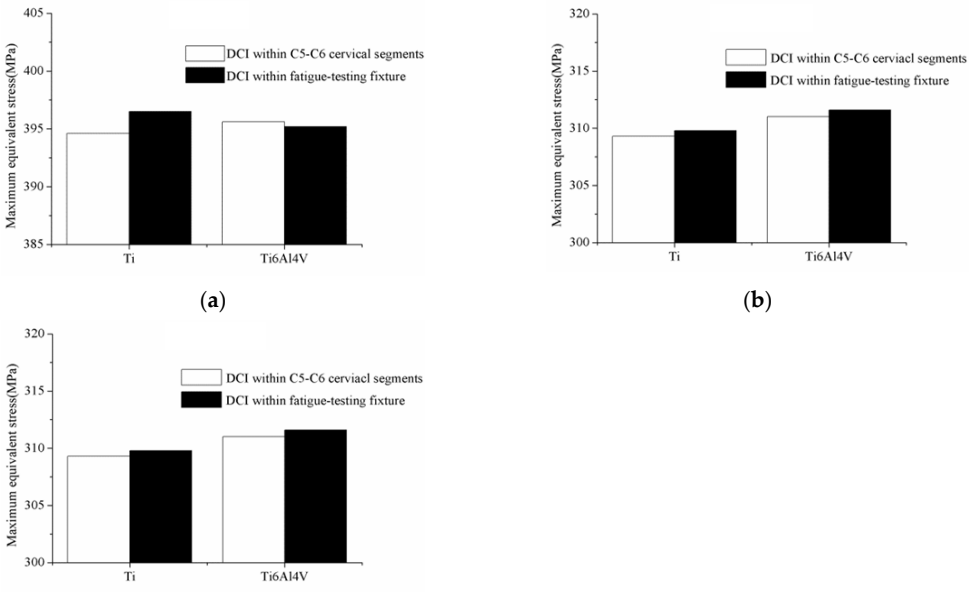

Figure 6. The maximum equivalent stress of DCI within C5–C6 cervical segments and within the fatigue-testing fixture in (**a**) flexion, (**b**) extension, and (**c**) lateral bending movements.

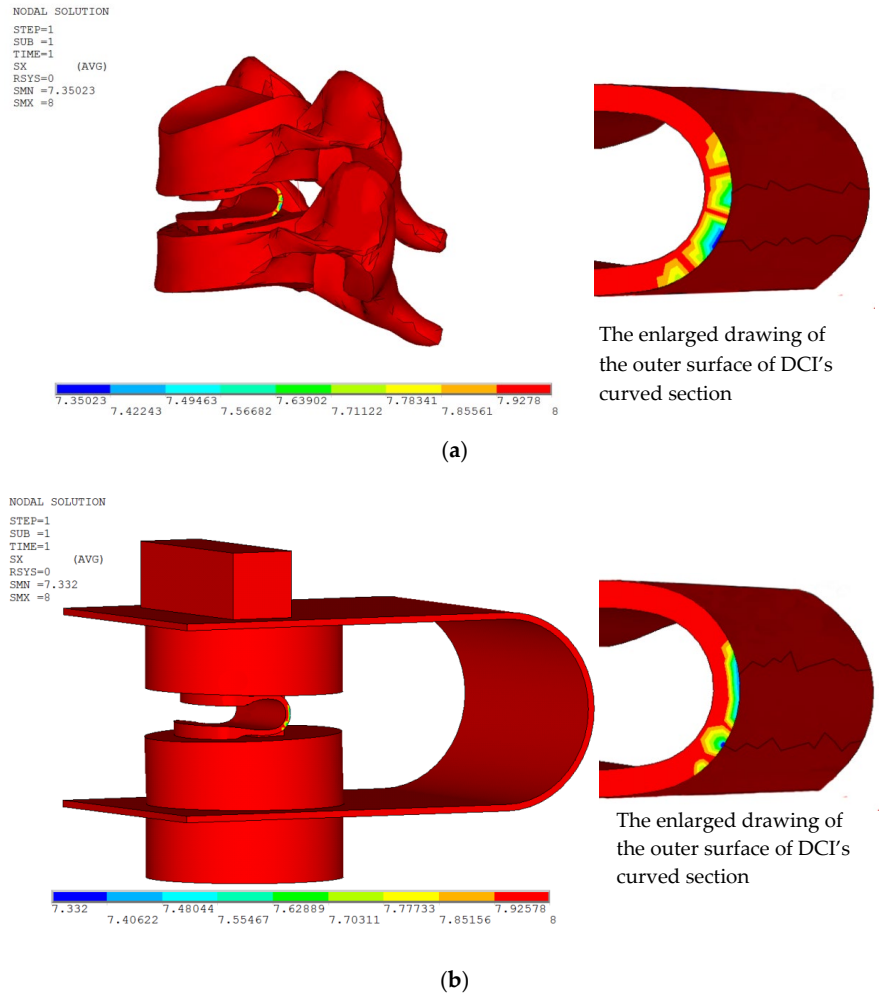

Figure 7. The contours of the fatigue life of pure Ti DCI under the flexion condition: (**a**) within C5–C6 cervical spinal segments; (**b**) within the fatigue-testing fixture.

Table 2. Simulated fatigue results and fatigue-testing results.

Type of Load	DCI Material	Simulated Fatigue Life of DCI within C5–C6 Cervical Spinal Segments (Million Cycles)	Simulated Fatigue Life of DCI within Fatigue-Testing Fixture (Million Cycles)	Fatigue-Testing Life of DCI within Fatigue-Testing Fixture (Million Cycles)
Flexion	Ti	22.397	21.478	35.645
	Ti6Al4V	≥80	≥80	≥80
Extension	Ti	≥80	≥80	≥80
	Ti6Al4V	≥80	≥80	≥80
Lateral bending	Ti	≥80	≥80	≥80
	Ti6Al4V	≥80	≥80	≥80

4. Discussion

Human physiological motion is complicated, comprehensive, and cooperative, which is difficult to represent accurately. However, its main functions are highlighted by mimicking the main biological structures and control principles of human cervical vertebrae.

4.1. The Rationality of the Static Load Settings

Notably, 200 N is also the routine maximum fatigue compressive force applied in the dynamic tests of ACDs according to ASTM F2346 [21,29,30]. In order to bridge the loading parameters in biomechanical tests with cervical spines from cadaver donors and in static and dynamic tests following ASTM F2346, an extra equivalent moment can be obtained by finely adjusting the eccentric distance between the centers of the cuboid block 01 and ACD during the finite element simulations of the static and fatigue experiments. For example, in the flexion movement, a 1.8 Nm flexion moment and 73.6 N preload with a 6 mm eccentric distance between the center of the implant position of ACD and the center of C5–C6 cervical spinal segments were applied onto the top surface of C5; therefore, the comprehensive loading moment was 73.6 N × 6 mm + 1.8 Nm = 2.242 Nm. According to ASTM F2346 test methods, a similar comprehensive load in the fatigue-testing fixture can be achieved (i.e., 200 N × 11.2 mm = 2.240 Nm) only by adjusting the eccentric distance between the force loading position (cuboid block 01) and the center of ACD to 11.2 mm [29,33]. Likewise, identical comprehensive loads can be obtained for either extension or lateral bending movements.

Meanwhile, the extra equivalent moment was also stable in the process of motion due to the tiny deformation of ACDs in the fatigue test. In consideration of experimental conditions and the various testing requirements of ACDs, the above loading methodology is not merely reasonable but also easily achieved.

4.2. Optimization of the Biomimetic Fatigue-Testing Fixture

When the elastic modulus of U-plate 05 reached 70,000 MPa, the deformation of the DCI was 0.57 mm, which is the same value as that of the DCI with human C5–C6 cervical spinal segments, as shown in Figure 3a. Among a variety of candidate materials, 6061 Al alloy was the most suitable. Simultaneously, the optimized thickness and width of the U-plate 05 were confirmed as 1 mm and 30 mm, respectively, according to Figure 3b,c. The geometric sizes of the cuboid block 01 and the cylindrical blocks 02–04 had no obvious influence on the DCI's maximum deformation, as shown in Figure 4. Therefore, the sizes of the blocks were determined according to those of the cervical vertebrae, while the distance between the center of the cylindrical blocks 02–04 and the rear end of the U-plate 05 should be inclined to that between the intervertebral disc and ligaments.

The optimized parameters of the biomimetic fatigue-testing fixture are as follows: 6061 Al alloy is suitable for the U-plate 05; the thickness and width of the U-plate 05 are 1 mm and 30 mm; the hydroxyapatite-filled epoxy block 01 is a 25 mm long, 10 mm wide and 10 mm high cuboid; the radius and height of the hydroxyapatite-filled epoxy cylindrical

blocks 02–04 are 12 mm and 10 mm; and the distance between the center of the cylindrical blocks 02–04 and the rear end of the U-plate 05 is 50~55 mm.

By employing these loading conditions and the optimized fixture, the simulated results of the maximum equivalent stress of the DCI within the C5–C6 cervical segments and within the fatigue-testing fixture present a series of consistencies in flexion, extension, and lateral bending movements, as shown in Figure 6.

4.3. The Safety of the Biomimetic Fatigue-Testing Fixture

The safety of the fixture is its foundation and premise during long periods of cyclic loading. The simulated fatigue lives of the U-plate and the blocks were more than 80 million cycles, as shown in Figure 7. Furthermore, the failure of the biomimetic fatigue-testing fixture did not occur in the 80-million-cycle fatigue experiments. Therefore, it can be concluded that the fixture is highly safe.

4.4. The Equivalence between the Biomimetic Fatigue-Testing Fixture and the Natural Cervical Sections

As shown in Figure 5, the curved section of the DCI is prone to forming crack sources due to large stresses; the cracks could propagate gradually during long periods of cyclic loading and finally cause the fatigue fracture of the DCI when the cyclic times accumulate beyond its fatigue life.

Under the circumstance that the equivalent stress and deformation of the DCI within C5–C6 cervical segments are almost the same as those within the biomimetic fatigue-testing fixture, the results of both fatigue simulations coincide well with the experimental results. The calculated fatigue lives of DCI within the C5–C6 cervical spinal segments and within the fatigue-testing fixture were 22.397 million cycles and 21.478 million cycles, respectively, which agree well with the experimental fatigue life of 35.645 million cycles, as shown in Table 2. It is noticeable that the simulated fatigue lives and possible sites for the fatigue failure of pure Ti DCI were almost same whether it was fixed within C5–C6 cervical spinal segments or within the fatigue-testing fixture, as shown in Figure 7.

In brief, the prostheses within the fatigue-testing fixture under the loads according to ASTM F2346 can achieve a functionally equivalent result to that under the biomechanical loads within normal cervical vertebrae.

4.5. Limitations of the Biomimetic Fatigue-Testing Fixture

The present study of biomimetic fatigue-testing fixtures has two limitations. Firstly, actual cervical movement includes not only flexion, extension, lateral bending, and axial torsion but also the combinations of single movement patterns within the scope of physiology. The biomechanical axial torsion and preload cannot be equivalent to the moment, which relates to the compressive force perpendicular to the surface of cuboid block 01, because they are not in a common plane. Therefore, the biomimetic fixture cannot meet the requirements for the torsion condition. Additionally, the biomimetic fatigue-testing fixture is only suitable for single load patterns, such as flexion, extension, and lateral bending. Unfortunately, single load patterns may be considered to be clinically unrealistic.

Secondly, muscle forces in spinal motions should not be neglected. Muscles in the loading spine generate spinal reaction forces, which can occupy the main portion of the total axial compression and shear forces on the spine, further affecting the life of ACD prostheses [34]. Simultaneously, posterior muscles can assist with balance in flexion postures; accordingly, anterior muscles act in the same role in extension postures. They can reduce the reaction forces of the lower joints and keep the spine steady [35]. These aspects are significant for ACD prostheses, especially when dynamic or impact loading is applied [36,37]. Unfortunately, synergism among the muscles is difficult to investigate because specimens in vitro cannot mimic the role of muscles well [34].

5. Conclusions

In summary, a novel specimen fixture has been designed for testing the fatigue behavior of ACD prostheses with aspects of both structural and functional bionics. The equivalence between the designed biomimetic fixture and the natural cervical sections has been verified by numerical simulations and mechanical experiments. This biomimetic fatigue-testing fixture represented the biomechanical characteristics of normal human cervical vertebrae with considerable accuracy. The novel specimen fixture provides a convenient and accurate way to research and evaluate the fatigue behavior of ACD prostheses.

Author Contributions: X.C., J.B. and T.W. contributed substantially to the conception and design of the experiments. X.C. and J.B. conducted experiments and wrote the manuscript. T.W. conducted data analyses. All authors have read and agreed to the published version of the manuscript.

Funding: This research was funded by the International Science and Technology Cooperation Programme (2018YFE0194100), the National Natural Science Foundation of China (51875231), and the Priority Academic Program Development of Jiangsu Higher Education Institutions.

Institutional Review Board Statement: Not applicable.

Informed Consent Statement: Not applicable.

Data Availability Statement: The original contributions presented in the study are included in the article; further inquiries can be directed to the corresponding author.

Conflicts of Interest: The authors declare no conflict of interest.

References

1. Hilibrand, A.S.; Robbins, M. Adjacent segment degeneration and adjacent segment disease: The consequences of spinal fusion? *Spine J.* **2004**, *4*, S190–S194. [CrossRef] [PubMed]
2. Matsumoto, M.; Okada, E.; Ichihara, D.; Watanabe, K.; Chiba, K.; Toyama, Y. Adjacent segment disease and degeneration after anterior cervical decompression and fusion. *Neurosurg. Q.* **2010**, *20*, 15–22. [CrossRef]
3. Fiani, B.; Nanney, J.M.; Villait, A.; Sekhon, M.; Doan, T. Investigational research: Timeline, trials, and future directions of spinal disc arthroplasty. *Cureus* **2021**, *13*, 16739. [CrossRef] [PubMed]
4. Joaquim, A.F.; Makhni, M.C.; Riew, K.D. Evidence-based use of arthroplasty in cervical degenerative disc disease. *Int. Orthop.* **2019**, *43*, 767–775. [CrossRef] [PubMed]
5. Lee, H.; Lee, M.; Han, G.; Kim, H.; Song, J.; Na, Y.; Yoon, C.; Oh, S.; Jang, T.; Jung, H. Customizable design of multiple-biomolecule delivery platform for enhanced osteogenic responses via 'tailored assembly system'. *Bio-Des. Manuf.* **2022**, *5*, 451–464. [CrossRef]
6. Lee, H.; Lee, M.; Cheon, K.; Kang, I.; Park, C.; Jang, T.; Han, G.; Kim, H.; Song, J.; Jung, H. Functionally assembled metal platform as lego-like module system for enhanced mechanical tunability and biomolecules delivery. *Mater. Design.* **2021**, *207*, 109840. [CrossRef]
7. Gloria, A.; Causa, F.; De Santis, R.; Netti, P.A.; Ambrosio, L. Dynamic-mechanical properties of a novel composite intervertebral disc prosthesis. *Mater. Med.* **2007**, *18*, 2159–2165. [CrossRef]
8. Rosa, G.L.; Clienti, C.; Corallo, D. Design of a new intervertebral disc prosthesis. *Mater. Today Proc.* **2019**, *7*, 529–536. [CrossRef]
9. Barker, J.B.; Cronin, D.S.; Chandrashekar, N. High rotation rate behavior of cervical spine segments in flexion and extension. *J. Biomech. Eng.* **2014**, *136*, 121004. [CrossRef]
10. Nuckley, D.J.; Linders, D.R.; Ching, R.P. Developmental biomechanics of the human cervical spine. *J. Biomech.* **2013**, *46*, 1147–1154. [CrossRef]
11. Lou, J.; Hao, L.; Li, Y.; Orthopedics, D.O.; Hospital, W.C.; University, S. Biomechanical evaluation of one new artificial cervical disc prosthesis. *Orthop. Biomech. Mater. Clin. Study* **2016**, *13*, 10–13.
12. Patwardhan, A.G.; Havey, R.M. Prosthesis design influences segmental contribution to total cervical motion after cervical disc arthroplasty. *Eur. Spine J.* **2020**, *29*, 2713–2721. [CrossRef]
13. Toen, C.V.; Melnyk, A.D.; Street, J.; Oxland, T.R.; Cripton, P.A. The Effects of Lateral Eccentricity on Failure Loads and Injuries of the Cervical Spine in Head-First Impacts. In Proceedings of the Ohio State University's 10th Annual Injury Biomechanics Symposium, Columbus, OH, USA, 18–20 May 2014; p. 18.
14. Rezaei, A.; Giambini, H.; Carlson, K.D.; Xu, H.; Lu, L. Mechanical testing setups affect spine segment fracture outcomes. *J. Mech. Behav. Biomed.* **2019**, *100*, 103399. [CrossRef]
15. Rahm, M.; Brooks, D.; Harris, J.; Hart, R.; Hughes, J.; Ferrick, B.; Bucklen, B. Stabilizing effect of the rib cage on adjacent segment motion following thoracolumbar posterior fixation of the human thoracic cadaveric spine: A biomechanical study. *Clin. Biomech.* **2019**, *70*, 217–222. [CrossRef]

16. Mannen, E.M.; Friis, E.A.; Sis, H.L.; Wong, B.M.; Cadel, E.S.; Anderson, D.E. The rib cage stiffens the thoracic spine in a cadaveric model with body weight load under dynamic moments. *J. Mech. Behav. Biomed.* **2018**, *84*, 258. [CrossRef] [PubMed]
17. Shen, F.H.; Woods, D.; Miller, M.; Murrell, B.; Vadapalli, S. Use of the dual construct lowers rod strains in flexion-extension and lateral bending compared to two-rod and two-rod satellite constructs in a cadaveric spine corpectomy model. *Spine J.* **2021**, *21*, 2104–2111. [CrossRef]
18. Holsgrove, T.P.; Miles, A.W.; Gheduzzi, S. The application of physiological loading using a dynamic, multi-axis spine simulator. *Med. Eng. Phys.* **2017**, *41*, 74–80. [CrossRef]
19. Phillips, F.M.; Geisler, F.H.; Gilder, K.M.; Reah, C.; Howell, K.M.; McAfee, P.C. Long-term outcomes of the us fda ide prospective, randomized controlled clinical trial comparing pcm cervical disc arthroplasty with anterior cervical discectomy and fusion. *Spine* **2015**, *40*, 674–683. [CrossRef] [PubMed]
20. Graham, J.; Estes, B.T. What standards can (and can't) tell us about a spinal device. *SAS J.* **2009**, *3*, 178–183. [CrossRef] [PubMed]
21. Mannen, E.M. Mechanical Testing of the Thoracic Spine and Related Implants. In *Mechanical Testing of Orthopaedic Implants*; Woodhead Publishing: Sawston, UK, 2017; pp. 143–160.
22. Cza, B.; Emm, C.; Hls, D.; Esc, D.; Bmw, D.; Ww, B.; Bo, C.B.; Eaf, D.; Deaa, E. Moment-rotation behavior of intervertebral joints in flexion-extension, lateral bending, and axial rotation at all levels of the human spine: A structured review and meta-regression analysis. *J. Biomech.* **2020**, *100*, 109579.
23. Sherrill, J.T.; Siddicky, S.F.; Davis, W.D.; Chen, C.; Mannen, E.M. Validation of a custom spine biomechanics simulator: A case for standardization. *J. Biomech.* **2019**, *98*, 109470. [CrossRef] [PubMed]
24. Mo, Z.J.; Zhao, Y.B.; Wang, L.Z.; Sun, Y.; Zhang, M.; Fan, Y.B. Biomechanical effects of cervical arthroplasty with u-shaped disc implant on segmental range of motion and loading of surrounding soft tissue. *Eur. Spine J.* **2014**, *23*, 613–621. [CrossRef] [PubMed]
25. Teo, E.C.; Ng, H.W. Evaluation of the role of ligaments, facets and disc nucleus in lower cervical spine under compression and sagittal moments using finite element method. *Med. Eng. Phys.* **2001**, *23*, 155–164. [CrossRef] [PubMed]
26. Vette, A.H.; Yoshida, T.; Thrasher, T.A.; Masani, K.; Popovic, M.R. A comprehensive three-dimensional dynamic model of the human head and trunk for estimating lumbar and cervical joint torques and forces from upper body kinematics. *Med. Eng. Phys.* **2012**, *34*, 640–649. [CrossRef]
27. Nimbarte, A.D.; Zreiqat, M.; Ning, X. Impact of shoulder position and fatigue on the flexion-relaxation response in cervical spine. *Clin. Biomech.* **2014**, *29*, 277–282. [CrossRef]
28. Cheng, X.; Wang, T.; Pan, C. Finite element analysis and validation of segments c2-c7 of the cervical spine. *Metals* **2022**, *12*, 2056. [CrossRef]
29. Kim, S.B.; Bak, K.H.; Cheong, J.H.; Kim, J.M.; Kim, C.H.; Oh, S.H. Biomechanical testing of anterior cervical spine implants: Evaluation of changes in strength characteristics and metal fatigue resulting from minimal bending and cyclic loading. *J. Korean Neurosurg. Soc.* **2005**, *37*, 217–222.
30. Bai, C.; Wei, W.; Hou, D. Biomechanical analysis of a new titanium rubber cervical disc prosthesis. *Chin. J. Spine Spinal Cord.* **2014**, *24*, 752–756.
31. Elder, J.E.; Thamburaj, R.; Patnaik, P.C. Optimising ion implantation conditions for improving wear, fatigue, and fretting fatigue of ti-6ai-4v. *Surf. Eng.* **1989**, *5*, 55–79. [CrossRef]
32. Kim, W.J.; Hyun, C.Y.; Kim, H.K. Fatigue strength of ultrafine-grained pure ti after severe plastic deformation. *Scripta Mater.* **2006**, *54*, 1745–1750. [CrossRef]
33. Espinoza-Larios, A.; Ames, C.P.; Chamberlain, R.H.; Sonntag, V.; Dickman, C.A.; Crawford, N.R. Biomechanical comparison of two-level cervical locking posterior screw/rod and hook/rod techniques. *Spine J.* **2007**, *7*, 194–204. [CrossRef]
34. Arjmand, N.; Gagnon, D.; Plamondon, A.; Shirazi-Adl, A.; Larivière, C. Comparison of trunk muscle forces and spinal loads estimated by two biomechanical models. *Clin. Biomech.* **2009**, *24*, 533–541. [CrossRef] [PubMed]
35. Toosizadeh, N.; Haghpanahi, M. Generating a finite element model of the cervical spine: Estimating muscle forces and internal loads. *Sci. Iran.* **2011**, *18*, 1237–1245. [CrossRef]
36. Li, Y.; Lewis, G. Influence of surgical treatment for disc degeneration disease at c5–c6 on changes in some biomechanical parameters of the cervical spine. *Med. Eng. Phys.* **2010**, *32*, 595–603. [CrossRef] [PubMed]
37. Panjabi, M.M.; Cholewicki, J.; Nibu, K.; Grauer, J.N.; Babat, L.B.; Dvorak, J. Mechanism of whiplash injury. *Clin. Biomech.* **1998**, *13*, 239–249. [CrossRef]